University of Reading

Mucoadhesive pickering nanoemulsions via dynamic covalent chemistry

Article

Published Version

Creative Commons: Attribution 4.0 (CC-BY)

Open Access

Hunter, S. J., Abu Elella, M. H., Johnson, E. C., Taramova, L., Brotherton, E. E., Armes, S. P., Khutoryanskiy, V. ORCID: https://orcid.org/0000-0002-7221-2630 and Smallridge, M. J. (2023) Mucoadhesive pickering nanoemulsions via dynamic covalent chemistry. Journal of Colloid and Interface Science, 651. pp. 334-345. ISSN 0021-9797 doi: https://doi.org/10.1016/j.jcis.2023.07.162 Available at https://centaur.reading.ac.uk/112840/

It is advisable to refer to the publisher's version if you intend to cite from the work. See Guidance on citing.

To link to this article DOI: http://dx.doi.org/10.1016/j.jcis.2023.07.162

Publisher: Elsevier

All outputs in CentAUR are protected by Intellectual Property Rights law, including copyright law. Copyright and IPR is retained by the creators or other copyright holders. Terms and conditions for use of this material are defined in the End User Agreement.

www.reading.ac.uk/centaur

University of Reading

CentAUR

Central Archive at the University of Reading

Reading's research outputs online

Journal of Colloid and Interface Science 651 (2023) 334–345

Contents lists available at ScienceDirect

Journal of Colloid And Interface Science

journal homepage: www.elsevier.com/locate/jcis

Mucoadhesive pickering nanoemulsions via dynamic covalent chemistry

Saul J. Hunter [a,1], Mahmoud H. Abu Elella [b,c,1], Edwin C. Johnson [a], Laura Taramova [b], Emma E. Brotherton [a], Steven P. Armes [a,*], Vitaliy V. Khutoryanskiy [b,*], Mark J. Smallridge [d]

[a] Dainton Building, Department of Chemistry, University of Sheffield, Brook Hill, Sheffield, South Yorkshire S3 7HF, UK
[b] Reading School of Pharmacy, University of Reading, Whiteknights, Reading RG6 6AD, UK
[c] Chemistry Department, Faculty of Science, Cairo University, Giza 12613, Egypt
[d] GEO Specialty Chemicals, Hythe, Southampton, Hampshire SO45 3ZG, UK

GRAPHICAL ABSTRACT

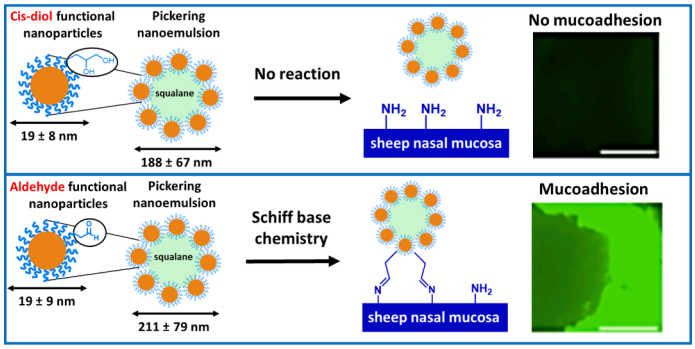

ARTICLE INFO

Keywords:
Nanoemulsions
Pickering emulsions
Block copolymers
Sterically-stabilized nanoparticles
Mucoadhesion
Schiff base chemistry
Aldehyde-functional

ABSTRACT

Hypothesis. Submicron oil droplets stabilized using aldehyde-functionalized nanoparticles should adhere to the primary amine groups present at the surface of sheep nasal mucosal tissue via Schiff base chemistry. *Experiments.* Well-defined sterically-stabilized diblock copolymer nanoparticles of 20 nm diameter were prepared in the form of concentrated aqueous dispersions via reversible addition-fragmentation chain transfer (RAFT) aqueous emulsion polymerization of 2,2,2-trifluoroethyl methacrylate (TFEMA) using a water-soluble methacrylic precursor bearing *cis*-diol groups. Some of these hydroxyl-functional nanoparticles were then selectively oxidized using an aqueous solution of sodium periodate to form a second batch of nanoparticles bearing pendent aldehyde groups within the steric stabilizer chains. Subjecting either hydroxyl- or aldehyde-functional nanoparticles to high-shear homogenization with a model oil (squalane) produced oil-in-water Pickering macroemulsions of 20–30 μm diameter. High-pressure microfluidization of such macroemulsions led to formation of the corresponding Pickering nanoemulsions with a mean droplet diameter of around 200 nm. Quartz crystal microbalance (QCM) experiments were used to examine adsorption of both nanoparticles and oil droplets onto a model planar substrate bearing primary amine groups, while a fluorescence microscopy-based mucoadhesion assay was developed to assess adsorption of the oil droplets onto sheep nasal mucosal tissue. *Findings.* Squalane droplets coated with aldehyde-functional nanoparticles adhered significantly more strongly to sheep nasal mucosal tissue

* Corresponding authors.
E-mail addresses: s.p.armes@sheffield.ac.uk (S.P. Armes), v.khutoryanskiy@reading.ac.uk (V.V. Khutoryanskiy).
[1] These authors contributed equally to this work.

https://doi.org/10.1016/j.jcis.2023.07.162
Received 18 April 2023; Received in revised form 29 June 2023; Accepted 26 July 2023
Available online 27 July 2023
0021-9797/© 2023 The Authors. Published by Elsevier Inc. This is an open access article under the CC BY license (http://creativecommons.org/licenses/by/4.0/).

than those coated with the corresponding hydroxyl-functional nanoparticles. This difference was attributed to the formation of surface imine bonds via Schiff base chemistry and was also observed for the two types of nanoparticles alone in QCM studies. Preliminary biocompatibility studies using planaria indicated only mild toxicity for these new mucoadhesive Pickering nanoemulsions, suggesting potential applications for the localized delivery of hydrophobic drugs.

1. Introduction

Pickering emulsions typically comprise oil, water and a (nano)particle emulsifier.[1–11] Known for more than a century, such emulsions offer superior long-term stability and minimal foaming problems compared to the equivalent surfactant-stabilized emulsions.[2,6,12,13] Many types of either inorganic or organic particles can be employed as Pickering emulsifiers.[14–20] The key parameter is the surface wettability, which in turn dictates the particle contact angle, θ. If θ is less than 90°, then the particles are hydrophilic and the formation of oil-in-water emulsions is favored. On the other hand, θ values above 90° are characteristic of hydrophobic particles, which usually lead to the stabilization of water-in-oil emulsions.

Pickering nanoemulsions have only been explored within the past decade.[21–32] Such systems comprise a much smaller droplet phase (typically < 200 nm diameter[33,34]) than that normally reported for Pickering emulsions (10–50 μm diameter).[5,17,35,36] In general, nanoemulsions are significantly less stable than emulsions. This is because the fine droplet size leads to a relatively high Laplace pressure, which drives diffusion of the oil (or water) molecules from smaller droplets through the continuous phase into larger droplets. This phenomenon is known as Ostwald ripening, which is the main instability mechanism exhibited by both surfactant-stabilized and Pickering nanoemulsions.[23,26,30,31,34,37–42] This problem can be suppressed (but not eliminated) by selecting an oil that is highly immiscible with water, which substantially reduces the rate of Ostwald ripening.[23,26,31,40,43] One reason why Pickering nanoemulsions have remained unexplored until recently is the relative lack of sufficiently small nanoparticles to stabilize such fine droplets. As a general rule of thumb, the particulate emulsifier should be at least 5–10 times smaller than the droplet diameter.[24] Thus, if a mean droplet diameter of 200 nm is desired, the nanoparticle emulsifier should have a mean diameter of 20–40 nm. Fortunately, a versatile platform technology known as polymerization-induced self-assembly (PISA)[44–50] has been developed that enables the rational synthesis of organic nanoparticles.

PISA involves the chain extension of a soluble precursor polymer to form a diblock copolymer using a suitable monomer that ensures the growing second block becomes insoluble in the chosen solvent. This inevitably leads to *in situ* self-assembly and a colloidal dispersion of sterically-stabilized diblock copolymer nanoparticles is obtained at the end of the polymerization. Moreover, PISA can be conducted in either water or various oils, which means that either hydrophilic or hydrophobic nanoparticles can be produced. The most common copolymer morphology is spheres,[51–53] which is well-suited for the design of Pickering nanoemulsions because sufficiently small nanoparticles can be readily prepared via PISA.

In principle, mucosal drug delivery offers several important advantages, including the ease of dosage form administration, non-invasiveness and improved bioavailability.[54] Established routes for transmucosal drug administration include ocular, nasal, oromucosal, gastrointestinal, vaginal and intravesical. Each route offers certain advantages, for example, nasal drug delivery provides an opportunity to target the brain.[55] Mucosal membranes are dynamic surfaces that are continuously reformed via secretion of mucins. Adhesion to mucosal surfaces is termed mucoadhesion and this phenomenon has been widely used to design drug formulations with improved retention characteristics, which in turn minimizes dosage requirements.[56,57]

Virtually all hydrophilic polymers adhere to mucosal surfaces to some extent owing to non-specific physical interactions such as electrostatic attraction, hydrogen bonding, and molecular entanglements.[58] These are known as first-generation mucoadhesives. However, certain therapeutic applications require enhanced mucoadhesion. In principle, this can be achieved using second-generation mucoadhesives based on functionalized polymers or particles that can form covalent bonds with mucins. Examples of suitable functional groups include thiols, (meth)acrylates, maleimides, phenylboronic acids, etc.[59,60]

Introduction of specific mucoadhesive groups can be achieved by functionalization of water-soluble polymers. Alternatively, colloidal particles can be prepared from functional small molecules.[61–63] An interesting strategy was recently reported by Edwards et al.,[64] who prepared mucoadhesive oil-in-water Pickering macroemulsions using thiol-functionalized branched copolymers as an emulsifier.

In the present study, we design new hydrophilic hydroxyl-functionalized diblock copolymer nanoparticles to act as an emulsifier for the preparation of oil-in-water Pickering nanoemulsions. In principle, such nanoemulsions can be used to formulate poorly water-soluble drugs. Squalane was selected as a highly water-insoluble biocompatible oil because it is known to mitigate the long-term instability associated with nanoemulsions via Ostwald ripening.[23,31] Recently, we reported that aldehyde-functional hydrogels – prepared via selective oxidation of precursor hydroxyl-functional hydrogels using sodium periodate – exhibit strong mucoadhesion to a model substrate (porcine urinary bladder mucosa).[65] Accordingly, the same synthetic methodology has been employed herein to convert the precursor hydroxyl-functionalized nanoparticles into aldehyde-functionalized nanoparticles. The mucoadhesive behavior of such aldehyde-functionalized nanoparticles and the corresponding Pickering nanoemulsions was examined using sheep nasal mucosal tissue as a model substrate. The precursor hydroxyl-functionalized nanoparticles (and corresponding Pickering nanoemulsions) were employed for control experiments.

2. Experimental

2.1. Materials

All reagents were used as received unless otherwise stated. GEO5MA monomer was synthesized by Dr C. P. Jesson at GEO Specialty Chemicals (Hythe, UK) as previously described.[1] 4,4′-Azobis(4-cyanopentanoic acid) (ACVA; >98%), 2,2,2-trifluorethyl methacrylate (TFEMA; 99%), sodium periodate ($NaIO_4$, ≥ 99.8%), squalane (98%), 2-(trimethylammonium)ethyl amine (99%), sodium cyanoborohydride ($NaCNBH_3$, 95%), 3-aminopropyltriethoxysilane (APTES; ≥98%), fluorescein isothiocyanate (FITC, ≥90.0%), low molecular weight chitosan (degree of acetylation = 75–85%), fluorescein isothiocyanate dextran (FITC-dextran, molecular weight = 3,000–5,000 g mol^{-1}), sodium fluorescein (≥95.0%), benzalkonium chloride (≥95.0%) and diethyl ether (≥99.8%) were purchased from Sigma-Aldrich (Gillingham, UK). 2-Cyano-2-propyl dithiobenzoate (CPDB, >97%) was purchased from Strem Chemicals Ltd (Cambridge, UK). d_4-Methanol and d_6-acetone were purchased from Goss Scientific Instruments Ltd (Cheshire, UK). Dimethylformamide (DMF, ≥99.5%) was purchased from Fisher Scientific (UK). Deionized water was used for all experiments involving aqueous solutions.

2.2. Methods

^{1}H NMR spectroscopy. Spectra were recorded in either d_4-methanol or d_6-acetone using a 400 MHz Bruker Avance-400 spectrometer at 298 K with 16 scans being averaged per spectrum.

DMF Gel Permeation Chromatography (GPC). DMF GPC was used to determine the number-average molecular weights (M_n) and dispersities (M_w/M_n) for all (co)polymers. The instrument set-up comprised two Agilent PL gel 5 μm Mixed-C columns and a guard column connected in series to an Agilent 1260 Infinity GPC system operating at 60 °C. The GPC eluent was HPLC-grade DMF containing 10 mmol LiBr at a flow rate of 1.0 mL min^{-1}, the copolymer concentration was typically 1.0% w/w and calibration was achieved using a series of ten near–monodisperse poly(methyl methacrylate) standards ranging from 1,080 g mol^{-1} to 905,000 g mol^{-1}. Chromatograms were analyzed using Agilent GPC/SEC software.

Dynamic Light Scattering (DLS). DLS studies were performed using a Malvern Zetasizer Nano-ZS instrument equipped with a 4 mW He-Ne laser (λ = 633 nm) operating at a fixed scattering angle of 173°. Copolymer dispersions were diluted to 0.1% w/w using deionized water prior to light scattering studies at 25 °C, with 2 min being allowed for thermal equilibrium prior to each measurement. The hydrodynamic z–average particle diameter was calculated via the Stokes-Einstein equation, which assumes perfectly monodisperse, non-interacting spheres. The polydispersity index (PDI) is expressed as a standard deviation that indicates the breadth of the particle size distribution, rather than the experimental error.

Aqueous Electrophoresis. Diblock copolymer nanoparticles were analyzed using a Malvern Zetasizer Nano ZS instrument equipped with a 4 mW He−Ne laser (λ = 633 nm) operating at a fixed scattering angle of 173°. Samples were diluted to 0.1% w/w using 1 mM KCl, with either dilute NaOH or HCl being used for pH adjustment as required. Zeta potentials (ζ) were calculated from the Henry equation using the Smoluchowski approximation.

Transmission Electron Microscopy (TEM). Copper/palladium TEM grids (Agar Scientific, UK) were coated in-house to yield a thin film of amorphous carbon and were subjected to a glow discharge for 30 s. Aqueous droplets of either copolymer dispersions (5.0 μL, 0.1% w/w) or nanoemulsions (5.0 μL, 1% v/v) were placed on freshly-treated grids for 1 min and then carefully blotted with filter paper to remove excess solution. An aqueous droplet of uranyl formate solution (5 μL, 0.75% w/w) was placed on each sample-loaded grid for 20 s and then blotted with filter paper to remove excess stain. This negative staining protocol was required to ensure sufficient electron contrast. Each grid was then carefully dried using a vacuum hose. Imaging was performed at 80 kV using an FEI Tecnai Spirit 2 microscope fitted with an Orius SC1000B camera.

Analytical Centrifugation. Droplet size distributions were assessed using a LUMiSizer analytical photocentrifuge (LUM GmbH, Berlin, Germany) operating at 20 °C. Measurements were conducted on diluted Pickering nanoemulsions (1.0% v/v squalane) in 2 mm path length polyamide cells, initially at 400 rpm for 200 profiles (allowing 10 s between each profile) and then at 4000 rpm for a further 800 profiles. The squalane droplet density was taken to be 0.81 g cm^{-3}.

Quartz Crystal Microbalance Studies (QCM). Quartz crystal microbalance sensors coated with a 50 nm silica overlayer (QSX 303, ~5 MHz fundamental frequency) were purchased from Q-Sense (Sweden). Each sensor was cleaned according to the manufacturer's instructions. This protocol involved (i) UV/O_3 treatment for 15 min (Bioforce UV/O_3 cleaner, ~9 mW cm^{-2}, λ = 254 nm), (ii) exposure to 2% w/w sodium dodecylsulfate solution for 30 min, (iii) copious rinsing with deionized water and drying under N_2, (iv) a final UV/O_3 treatment for 15 min. The resulting sensors were then amine-functionalized at room temperature via exposure to APTES vapor (< 5 mbar) for 30 min.

QCM measurements were performed using an openQCM NEXT instrument (Novatech Srl., Italy) equipped with a temperature-controlled cell connected to a Masterflex Digital Miniflex peristaltic pump (Cole-Parmer Instrument Company, UK). All experiments were conducted using MilliQ water (pH 6) and were not commenced until the sensor frequency exhibited a drift of less than 0.1 Hz min^{-1}; this typically occurred within an hour of filling the cell. Once a stable signal was obtained, a 0.1% w/w aqueous dispersion of nanoparticles [or a 0.1% w/w squalane-in-water Pickering nanoemulsion] was passed through the cell at a flow rate of 0.025 mL min^{-1} (minimum flow volume = 2.0 mL).

From such QCM experiments, the adsorbed amount can be calculated using the Sauerbrey equation, which relates the change in frequency, Δf, directly to the change in adsorbed mass per unit area, m,[66–68]

$$m = C \times \frac{\Delta f}{n}$$

where C is a sensitivity constant (−0.177 (mg × m^{-2}) × Hz^{-1}), Δf is the change in resonant frequency (Hz), and n is the overtone number. The third harmonic (n = 3) was used to calculate the adsorbed amount to avoid experimental artifacts associated with the fundamental harmonic that may occur if the sample mounting on the sensor is imperfect. [66–68]

Atomic force microscopy (AFM). AFM imaging was performed using a Bruker Nanoscope™ VIII Multimode Atomic Force Microscope equipped with a 'J' scanner and a silicon cantilever (TESTPA-V2, Bruker, UK) with a nominal spring constant of 42 N•m^{-1} and tip radius of 7 nm. APTES coated silicon wafers were prepared as above. Nanoparticle adsorption was achieved by immersing an APTES-coated silicon wafer into a 1.0% w/w nanoparticle dispersion overnight, followed by copious rinsing with deionized water (pH 6) and drying under a stream of N_2 gas. The dried nanoparticle-decorated wafer was imaged in tapping mode at 24 °C. A second-order plane fit and second-order flattening was applied to process the resulting images.

2.3. Synthesis details

Synthesis of the PGEO5MA$_{26}$ precursor. PGEO5MA$_{26}$ was synthesized by RAFT solution polymerization of GEO5MA in ethanol using a previously described protocol.[2] Briefly, GEO5MA monomer (0.131 mol, 50.0 g), CPDB RAFT agent (0.882 g, 3.98 mmol), ACVA initiator (0.223 g, 0.797 mmol; CPDB/ACVA molar ratio = 5.0) and ethanol (34.0 g) were weighed into a 250 mL round–bottom flask. The reaction mixture was degassed for 40 min using a N_2 purge before being placed into an oil bath set at 70 °C for 110 min. The polymerization was quenched by removing the flask from the oil bath with concomitant exposure of the reaction mixture to air. The GEO5MA conversion was determined to be 58% by ^{1}H NMR spectroscopy. The crude PGEO5MA homopolymer was purified by precipitation into diethyl ether (to remove any unreacted monomer and other impurities), before being filtered and redissolved in methanol. This precipitation step was repeated and the purified homopolymer was dried in a vacuum oven set at 35 °C overnight to produce a red viscous liquid. The mean degree of polymerization (DP) of this PGEO5MA$_{26}$ precursor was determined by end-group analysis using ^{1}H NMR spectroscopy (the integrated signals between 7.34 and 8.03 ppm assigned to the five aromatic protons of the dithiobenzoate chain-end were compared to that of the five proton signals assigned to the methacrylate backbone at 0.78 – 2.71 ppm).

Synthesis of PGEO5MA$_{26}$-PTFEMA$_{35}$ nanoparticles. PGEO5MA$_{26}$-PTFEMA$_{35}$ nanoparticles were prepared by chain-extending a PGEO5MA$_{26}$ precursor with TFEMA (target DP = 35) via RAFT aqueous emulsion polymerization of TFEMA at 70 °C, using the protocol reported by Akpinar and co-workers for the synthesis of closely-related diblock copolymer nanoparticles.[52] After 18 h, the TFEMA polymerization was quenched by exposing the reaction solution to air while cooling to 20 °C. ^{19}F NMR spectroscopy analysis of the resulting PGEO5MA$_{26}$-PTFEMA$_{35}$ chains dissolved in d_6-acetone indicated less than 1%

residual TFEMA monomer. These nanoparticles were used without further purification.

Selective oxidation of PGEO5MA$_{26}$-PTFEMA$_{35}$ nanoparticles using sodium periodate. Sodium periodate (0.120 g, 0.540 mmol) was dissolved in a 10% w/w aqueous dispersion of PGEO5MA$_{26}$-PTFEMA$_{35}$ nanoparticles (4.50 g, 21.0 μmol). A $NaIO_4$/*cis*-diol molar ratio of unity was used to target 100% oxidation of the *cis*-diol units within the PGEO5MA block. The reaction solution was stirred in the dark for 30 min at 22 °C. The mean degree of oxidation was determined to be 100% by ^{1}H NMR spectroscopy. The resulting PAGEO5MA$_{26}$-PTFEMA$_{35}$ nanoparticles were dialyzed against deionized water for two days prior to use.

Derivatization of PAGEO5MA$_{26}$ homopolymer with 2-(trimethylammonium)ethyl amine. PAGEO5MA$_{26}$ (1.00 g of a 10% w/w aqueous solution) and 2-(trimethylammonium)ethyl amine (0.29 mmol, 50.0 mg) were weighed into a 15 mL sample vial. A 2-(trimethylammonium)ethyl amine/aldehyde molar ratio of unity was used and the reaction mixture was stirred at 35 °C for 48 h to ensure full conversion of aldehyde to the corresponding the imine intermediate. The resulting aqueous solution of 2-(trimethylammonium)ethyl imine-functionalized PAGEO5MA$_{26}$ was purified by dialysis against deionized water for two days (with at least three water changes per day) prior to analysis by ^{1}H NMR spectroscopy.

Reductive amination of PGEO5MA$_{26}$-PTFEMA$_{35}$ nanoparticles with 2-(trimethylammonium)ethyl amine. PGEO5MA$_{26}$-PTFEMA$_{35}$ nanoparticles (1.00 g of a 10% w/w aqueous solution), 2-(trimethylammonium)ethyl amine (0.12 mmol, 21.3 mg) and $NaCNBH_3$ (0.30 mmol, 18.7 mg) were weighed into a 15 mL sample vial. A 2-(trimethylammonium)ethyl amine/aldehyde molar ratio of unity was employed in combination with a 2.45-fold excess of $NaCNBH_3$. The reaction mixture was stirred at 35 °C for 48 h to ensure full conversion of aldehyde to the corresponding secondary amine via the imine intermediate. The resulting aqueous dispersion of 2-(trimethylammonium)ethyl amine-functionalized nanoparticles was purified by dialysis against deionized water for two days (with at least three water changes per day) prior to aqueous electrophoresis studies.

Preparation of PGEO5MA$_{26}$-PTFEMA$_{35}$-stabilized Pickering macroemulsions. An aqueous dispersion of either PGEO5MA$_{26}$-PTFEMA$_{35}$ or PAGEO5MA$_{26}$-PTFEMA$_{35}$ nanoparticles (4.0 mL, 7.0% w/w) was added to squalane (1.0 mL) in a 14 mL glass vial. This immiscible mixture was then subjected to high-shear homogenization for 2.0 min at 20 °C using an IKA Ultra-Turrax T-18 homogenizer operating at 13 500 rpm and equipped with a 10 mm dispersing tool. The resulting Pickering macroemulsion had a squalane volume fraction of 0.20 and a volume-average droplet diameter of 32 ± 24 μm. The same protocol was used to prepare the corresponding PAGEO5MA$_{26}$-PTFEMA$_{35}$-stabilized Pickering macroemulsion, which had a volume-average droplet diameter of 18 ± 11 μm.

Preparation of a PGEO5MA$_{26}$-PTFEMA$_{35}$-stabilized Pickering nanoemulsion via microfluidization. A Pickering macroemulsion (5.0 mL, initial nanoparticle concentration in the aqueous phase = 7.0% w/w, squalane volume fraction = 0.20) was further processed using an LV1 high-pressure microfluidizer (Microfluidics, USA). Each macroemulsion was passed ten times through the LV1 unit at an applied pressure of 20 000 psi to produce well-defined Pickering nanoemulsions. The same protocol was used to prepare the corresponding PAGEO5MA$_{26}$-PTFEMA$_{35}$-stabilized Pickering nanoemulsion.

In vitro nasal mucoadhesion study. The retention of either aldehyde- or hydroxyl-functionalized Nile Red-labeled squalane droplets on freshly-excised sheep nasal mucosal tissue was investigated using a flow-through fluorescence microscopy technique.[61,62] The tissue was irrigated with artificial nasal fluid (ANF). FITC-chitosan and FITC-dextran were employed as positive and negative controls, respectively.

Preparation of artificial nasal fluid (ANF). Artificial nasal fluid (ANF) was prepared according to previously published protocols.[69,70] Briefly, NaCl (7.45 g), $CaCl_2{\cdot}2H_2O$ (0.32 g) and KCl (1.29 g) were dissolved in ultrapure water (1000 mL) and stirred continuously overnight at room temperature. The resulting ANF was adjusted to pH 5.7 and this solution was stored at 37 °C prior to the mucoadhesion experiments.

Preparation of fluorescently-labeled chitosan and dextran. Fluorescently-labeled chitosan (FITC-Ch) was prepared using a previously published protocol.[63] Chitosan (Ch, 1.00 g) was dissolved in 1.0% acetic acid (100 mL) and stirred continuously overnight at ambient temperature. FITC (100 mg) was dissolved in methanol (50 mL) for 1 h and this solution was subsequently added to the acidic chitosan solution in the dark. The resulting reaction mixture was stirred at ambient temperature and after 3 h the FITC-Ch was precipitated into 0.1 M NaOH (1000 mL). This precipitate was isolated via filtration and then purified by dialysis against deionized water (5000 mL) in the dark for 72 h (with nine changes of water) using a cellulose membrane with a molecular weight cut-off of 12–14 kDa. After dialysis, the purified aqueous solution was placed in a round-bottom flask, frozen using liquid nitrogen and lyophilized overnight using a Heto Power Dry LL 3000 freeze-drier (with the flask being covered with aluminum foil to prevent UV degradation). For mucoadhesion studies, FITC-Ch (1.0 mg) was dissolved in 1.0% acetic acid (1.0 mL) while FITC-dextran (1.0 mg) was dissolved in deionized water (1.0 mL) and stirred continuously for 5 h at ambient temperature. For all experiments, the solution pH was adjusted to 5.7 using 0.1 M NaOH and/or 0.1 M HCl before performing retention studies using nasal mucosal tissue, as described below.

Retention studies using sheep nasal mucosa. In this study, fresh sheep heads were received from P.C. Turner Abattoir (Farnborough, UK) and used within 24 h of animal slaughter. Sections of nasal septum mucosal tissue (1.5 × 2.0 cm^2) were dissected using a disposable sharp blade, placed on a microscope glass slide and then washed with 2.0 mL of the ANF solution. All retention experiments were performed in an incubator at 37 °C using Nile Red-labeled squalane droplets, FITC-Ch (positive control) or FITC-dextran (negative control). Fluorescence images of nasal mucosal tissues were recorded using a fluorescence microscope (A Leica MZ10F Microsystems, UK) equipped with a Zeiss Imager A1/AxioCam MRm camera. All fluorescence images for the Nile Red-labeled nanoemulsion experiments were recorded using an ET CY3 filter at 2.0x magnification using an exposure time of 368 ms, a gain of 2.4, and a gamma of 1.6. For the FITC-Ch and FITC-dextran control experiments, fluorescence images were recorded using an exposure time of 160 ms, a gain of 1.0x and a gamma of 1.0x using an ET GFP filter. Nasal mucosa images recorded in the absence of any samples were used to determine the background fluorescence intensity. Then each sample (75 μL) was loaded in turn onto a nasal mucosal surface and transferred into a sloped channel to wash with ANF using a syringe pump operating at a flow rate of 1.0 mL min^{-1}. Fluorescence images were recorded at various time points and all experiments were performed in triplicate. All fluorescence images were analysed using ImageJ software to determine the fluorescence intensity remaining after each wash.

2.4. Toxicological studies

Acute toxicity assay in planaria. A toxicological evaluation of the two squalane-in-water nanoemulsions prepared using either aldehyde- or hydroxyl-functionalized nanoparticles was performed using *Schmidtea mediterranea* planaria according to our previously published protocol [71] with a few modifications. Planaria were kindly provided by Dr Jordi Solana (Oxford Brookes University) and kept in artificial pond water (APW) prior to use. APW was prepared by mixing 5.0 M NaCl (3.2 mL), 1.0 M $CaCl_2{\cdot}6H_2O$ (10.0 mL), 1.0 M $MgSO_4$ (10.0 mL), 1.0 M $MgCl_2$ (1.0 mL) and 1.0 M KCl (1.0 mL). This mixture was used to dissolve $NaHCO_3$ (1.008 g) and was subsequently diluted with ultrapure water (10 L). Each nanoemulsion was diluted to either 1.0 g dm^{-3} or 0.5 g dm^{-3} using APW and then filtered using a 0.45 μm syringe filter prior to each toxicity assay. Then each diluted nanoemulsion (1.0 mL) was added to every well in a 24-well plate and a single planarian worm was added to each well. All experiments were conducted in triplicate. APW was employed as a negative control and benzalkonium chloride (BC) dissolved in APW at either 0.5 or 1.0 g dm^{-3} was used as a positive

control. The toxicity of all samples towards planaria was assessed over 48 h at room temperature by monitoring the viability of this organism.

Planarian toxicity fluorescent assay. Planarian toxicity of the two nanoemulsions (0.5 mg/mL and 1.0 mg/mL), as well as BC in APW (positive control) and APW as a negative control, was conducted according to our previously published protocol[71] with some modifications. Planaria used for the 48 h acute toxicity assay were washed with APW for 1 min. Then each planarian was immersed for 1 min in 0.1% w/v sodium fluorescein (NaFl) dissolved in APW and then washed for 1 min using APW (15 mL) to remove excess NaFl. Each planarian was immobilized on a microscope glass slide using a few drops of 12% gelatin solution and then placed immediately on ice for 5 min. Experiments with planaria exposed to a positive control were performed using BC concentrations of 0.1 g dm^{-3}, 0.5 g dm^{-3} and 1.0 g dm^{-3} for contact times of 1 min, 1 h, 24 h and 48 h. Employing a BC concentration of either 0.5 or 1.0 g dm^{-3} in such experiments resulted in rapid intake of sodium fluoresceine into the planarium, which led to overexposed images that could not be analyzed quantitatively (see later). Therefore, a modified protocol was developed using a BC concentration of 0.1 g dm^{-3} and a contact time of 1 min per worm. This protocol produced higher quality fluorescence images, which were recorded using a Leica fluorescence microscope equipped with an ET GFP filter using an exposure time of 970 ms at 2.0× magnification, 5.1× gain, and 0.7× gamma. *ImageJ* software was used to quantify the fluorescence intensity within each planarian. These intensities were then normalized by dividing by the surface area (cm^2) of each planarian. All experiments were performed in triplicate.

Statistical analysis. All experiments were conducted in triplicate and data were expressed as mean ± standard deviation, with $p < 0.05$ taken to be a statistically significant difference. GraphPad Prism v9.0 software was used for statistical analysis and one-way ANOVA was performed to analyse the data.

3. Results and discussion

A $PGEO5MA_{26}$ precursor was prepared via RAFT solution polymerization of GEO5MA in ethanol using a non-ionic CPDB RAFT agent as shown in Figure S1. This homopolymer had an M_n of 14 300 g mol^{-1} and an M_w/M_n of 1.18, according to DMF GPC analysis using a series of poly(methyl methacrylate) calibration standards (see Figure S3). Subsequently, this water-soluble PGEO5MA precursor was chain-extended via RAFT aqueous emulsion polymerization of TFEMA at 70 °C targeting 10% w/w solids, as shown in Figure 1.

More than 99% TFEMA conversion was achieved after 18 h as judged by ^{19}F NMR spectroscopy (see Figure S2). DMF GPC analysis indicated reasonably good RAFT control, with an M_w/M_n of 1.28 and relatively high blocking efficiencies (see Figure S3). The $PGEO5MA_{26}$-$PTFEMA_{35}$ nanoparticles formed an almost transparent, free-flowing dispersion and a spherical morphology was confirmed by TEM studies. It is perhaps worth mentioning that a non-ionic RAFT agent was selected for this study. This is because ionic RAFT agents confer charged end-groups on the steric stabilizer chain, which is known to reduce the extent of nanoparticle adsorption at the oil–water interface.[42,72]

Recently, we reported that sodium periodate can selectively oxidize the pendant *cis*-diol units on the steric stabilizer chains to confer aldehyde functionality without loss of water solubility. Since aldehydes can react readily with amines via Schiff base chemistry,[73] such nanoparticles are expected to be mucoadhesive.[65] Moreover, such hydrophilic nanoparticles should enable the formation of mucoadhesive oil-in-water Pickering nanoemulsions. Accordingly, the steric stabilizer chains on the $PGEO5MA_{26}$-$PTFEMA_{35}$ nanoparticles were oxidized using a periodate/*cis*-diol molar ratio of 1.0 using a previously reported protocol.[74] ^1H NMR spectroscopy studies confirmed that full oxidation of the *cis*-diol groups was achieved within 30 min at 22 °C (see Figure S4). Unfortunately, the single aldehyde proton signal is rather weak and hence difficult to identify by ^1H NMR spectroscopy. Thus the

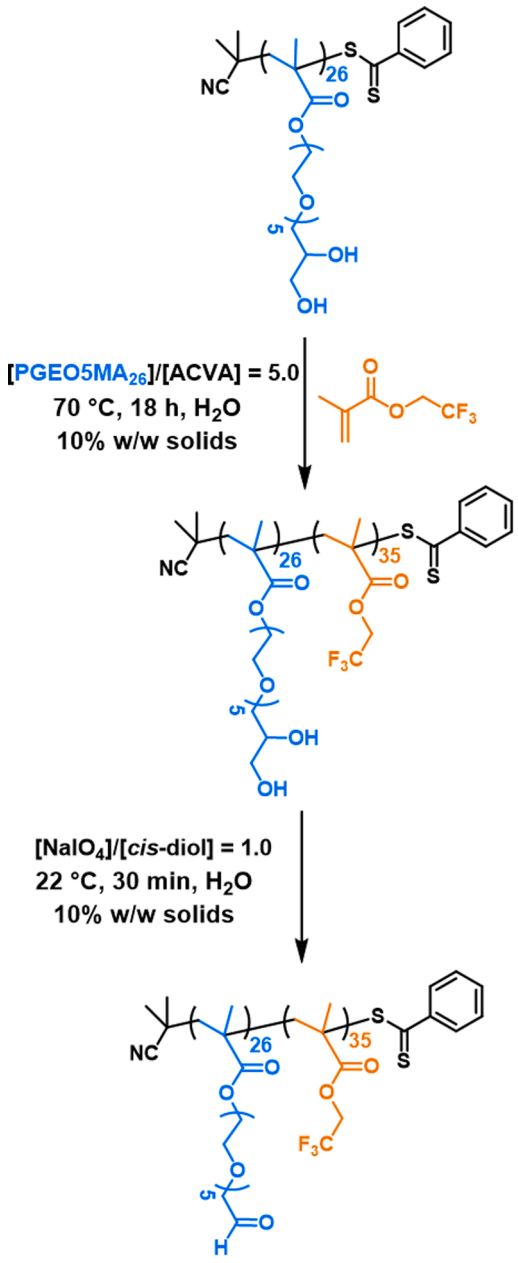

Fig. 1. Schematic representation of the two-step synthesis of aldehyde-functionalized $PAGEO5MA_{26}$–$PTFEMA_{35}$ diblock copolymer nanoparticles starting from a $PGEO5MA_{26}$ precursor. Initially, this water-soluble homopolymer is chain-extended via RAFT aqueous emulsion polymerization of TFEMA at 70 °C to form hydroxyl-functional $PGEO5MA_{26}$-$PTFEMA_{35}$ nanoparticles. The pendent *cis*-diol groups on the $PGEO5MA_{26}$ stabilizer chains are then selectively oxidized using aqueous sodium periodate at 22 °C.

$PGEO5MA_{26}$ precursor was reacted with stoichiometric amount of (i) $NaIO_4$ and (ii) 2-(trimethylammonium)ethyl amine at pH 9 to form an imine bond.[73] After dialysis against water to remove spent reagents, such derivatization produces a relatively strong trimethylammonium proton signal at 3.10 ppm (see Figure S5a-c). Furthermore, aqueous electrophoresis data (see Figure S5d) were obtained for $PGEO5MA_{26}$-$PTFEMA_{35}$ nanoparticles before (red data points) and after (black data points) their successive reaction with (i) a stoichiometric amount of $NaIO_4$ at 22 °C, (ii) a stoichiometric amount of 2-(trimethylammonium) ethyl amine at pH 9 and (iii) $NaCNBH_3$. In the former case, zeta potentials remain close to zero regardless of the solution pH. In contrast, highly cationic zeta potentials are observed across the whole pH range in

the latter case. Such experiments provide strong evidence that periodate treatment of the PGEO5MA$_{26}$-PTFEMA$_{35}$ nanoparticles introduces pendent aldehyde groups within the steric stabilizer chains.

GPC studies indicated that periodate treatment causes minimal change in the diblock copolymer molecular weight distribution (see Figure S2). Moreover, there was no discernible change in copolymer morphology after oxidation, with DLS reporting a z-average diameter of 19 ± 8 nm for the hydroxyl-functional PGEO5MA$_{26}$-PTFEMA$_{35}$ nanoparticles and 19 ± 9 nm for the corresponding aldehyde-functional PAGEO5MA$_{26}$-PTFEMA$_{35}$ nanoparticles. Similarly, number-average diameters of 17 ± 2 nm and 17 ± 3 nm were estimated for the PGEO5MA$_{26}$-PTFEMA$_{35}$ and PAGEO5MA$_{26}$-PTFEMA$_{35}$ nanoparticles based on TEM studies (at least 150 nanoparticles being analyzed in each case), as shown in Figure 2. Both types of nanoparticles bear hydrophilic steric stabilizer chains and hence are expected to exhibit particle contact angles of less than 90°.[20]

A two-step protocol was used to prepare squalane-in-water Pickering nanoemulsions using either the hydroxyl-functionalized PGEO5MA$_{26}$-PTFEMA$_{35}$ or the aldehyde-functional PAGEO5MA$_{26}$-PTFEMA$_{35}$ nanoparticles. This approach was based on a protocol developed by Thompson and co-workers[24] for the preparation of *n*-dodecane-in-water Pickering nanoemulsions using PGMA$_{48}$-PTFEMA$_{50}$ nanoparticles with a similar z-average diameter of 25 nm. Thus, squalane was added to a 7.0% w/v aqueous dispersion of PGEO5MA$_{26}$-PTFEMA$_{35}$ nanoparticles and the resulting immiscible mixture was subjected to high-shear homogenization to produce squalane-in-water Pickering macroemulsions with a mean droplet diameter of around 20–30 μm according to laser diffraction studies (see Figure S6). Such precursor macroemulsions were then processed using a commercial LV1 microfluidizer to produce Pickering nanoemulsions (see Figure 3). Empirically, Thompson and co-workers found that a relatively high nanoparticle concentration of around 7.0% w/w was required to produce oil droplets of around 200 nm diameter. Furthermore, multiple passes through the microfluidizer unit at an applied pressure of 20 000 psi were required. Lower pressures merely led to larger and more polydisperse droplets, whereas higher pressures led to *in situ* disintegration of the diblock copolymer nanoparticles to produce amphiphilic copolymer chains. DLS studies of the Pickering nanoemulsions generated using this protocol indicated the formation of squalane droplets with a z-average diameter of either 187 ± 67 nm or 211 ± 79 nm when using the hydroxyl-functional or aldehyde-functional nanoparticles, respectively (see Figure S7). Representative unimodal cumulative size distributions recorded for these two freshly-prepared Pickering nanoemulsions via analytical centrifugation are also shown in Figure S7. The hydroxyl-functional nanoparticles exhibit a volume-average diameter of 198 ± 120 nm while the aldehyde-functional nanoparticles possess a volume-average diameter of 231 ± 151 nm. Clearly, selective oxidation of the former nanoparticles using sodium periodate does not affect their ability to stabilize such Pickering nanoemulsions.

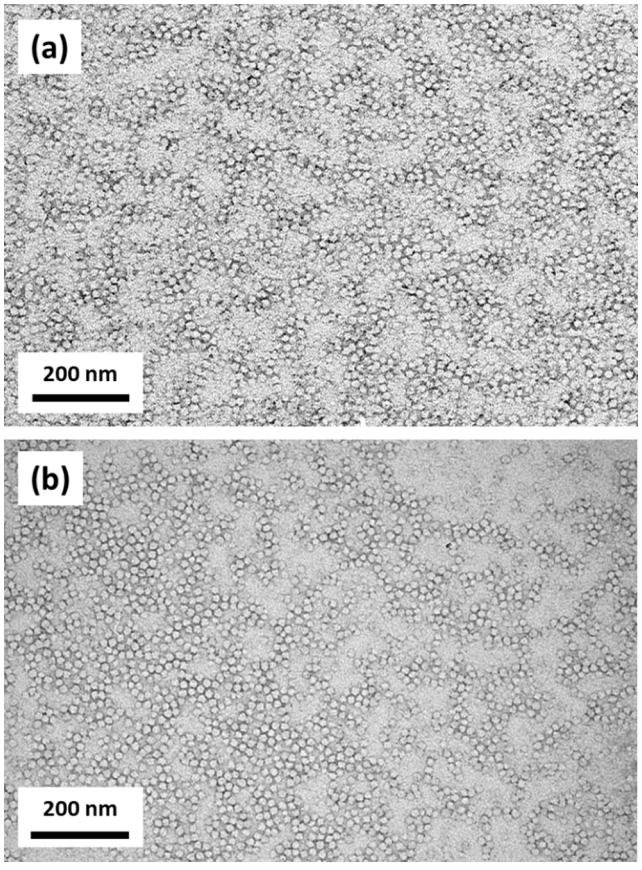

Fig. 2. Representative TEM images obtained for (a) hydroxyl-functional PGEO5MA$_{26}$-PTFEMA$_{35}$ nanoparticles and (b) aldehyde-functional PAGEO5MA$_{26}$-PTFEMA$_{35}$ nanoparticles.

In order to determine whether these nanoparticles survive the high-pressure microfluidization conditions, freshly-prepared Pickering nanoemulsions were dried for TEM studies, see Figure 4. The squalane and water are both evaporated under the ultrahigh vacuum conditions required for TEM, leaving behind the nanoparticle superstructure that surrounded the original oil droplets. Such *postmortem* studies confirm the presence of intact nanoparticles, indicating the formation of genuine Pickering nanoemulsions in both cases. Moreover, only a few non-adsorbed nanoparticles are visible in each case, suggesting a relatively high nanoparticle adsorption efficiency on the oil droplets.[42] Furthermore, analytical centrifugation studies confirmed minimal change in the droplet size distributions for both nanoemulsions after aging for four months at 20 °C (data not shown).

Quartz crystal microbalance (QCM) is an established analytical technique for monitoring the adsorption of various types of nanoparticles onto model planar substrates.[66,75–84] For example, the adsorbed mass of both spherical silica and disk-like Laponite nanoparticles onto an oppositely-charged surface has been reported by Biggs and co-workers.[80] In all cases, the observed reduction in the resonant frequency of the quartz crystal is converted into an adsorbed mass using the Sauerbrey equation. The calculated adsorbed mass includes both the solid adsorbed amount and any immobilized solvent within the adsorbed layer. As far as we are aware, there are rather few QCM studies of the adsorption of diblock copolymer nanoparticles onto model planar substrates.[83–85] This omission is perhaps surprising given the surge of interest in PISA syntheses of such sterically-stabilized nanoparticles over the past decade or so. The QCM data obtained in the present study are shown in Figure 5.

QCM studies of the adsorption of both types of nanoparticles and the corresponding squalane droplets were performed using commercial silica sensors that had been pre-treated with APTES to produce a model primary amine-functionalized substrate. Duplicate measurements were conducted for each adsorption experiment (Figure S8), with the adsorbed amount, Γ, calculated from the mean Δf value (Figure 5).

A reduction in the sensor frequency indicates the interfacial adsorption of either the nanoparticles or the nanoparticle-coated oil droplets. Then the sensor is subjected to a 'wash-off 'step using deionized water to remove any weakly adsorbed material, which invariably leads to a modest increase in Δf. Comparison of the raw Δf vs. time plots (Figure S8) indicates a significantly greater overall change in Δf for the nanoparticle-coated oil droplets compared to the corresponding nanoparticles alone. Moreover, both the aldehyde-functional nanoparticles and the corresponding oil droplets adsorbed much more strongly than the equivalent hydroxyl-functional nanoparticles or oil droplets.

The overall change in frequency after the 'wash-off' step is used to calculate Γ, as summarized in Figure 5. Clearly, the aldehyde-functional nanoparticles adsorb much more strongly onto the model aminated

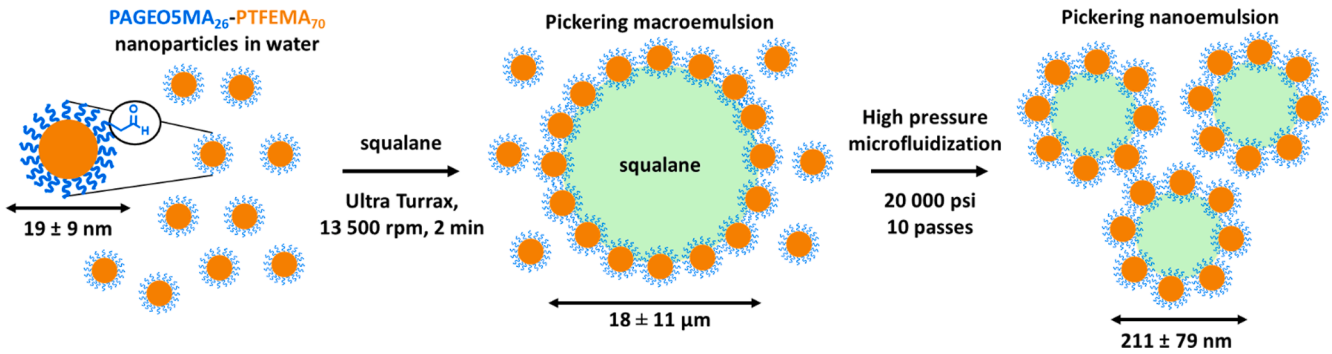

Fig. 3. Schematic representation of the two-stage preparation of Pickering nanoemulsions using 20 nm aldehyde-functional nanoparticles. First, a squalane-in-water Pickering macroemulsion of around 20–30 μm diameter is prepared by subjecting a 7.0% w/v aqueous dispersion of PAGEO5MA$_{26}$-PTFEMA$_{35}$ nanoparticles to high-shear homogenization with squalane at 13 500 rpm for 2 min at 20 °C. Subsequently, Pickering nanoemulsions of approximately 200 nm diameter were obtained by refining such coarse precursor Pickering macroemulsions via ten passes through a commercial LV1 microfluidizer at an applied pressure of 20 000 psi. The same approach and processing conditions was also used to prepare a hydroxyl-functional Pickering nanoemulsion using the hydroxyl-functional PGEO5MA$_{26}$-PTFEMA$_{35}$ nanoparticles for control experiments.

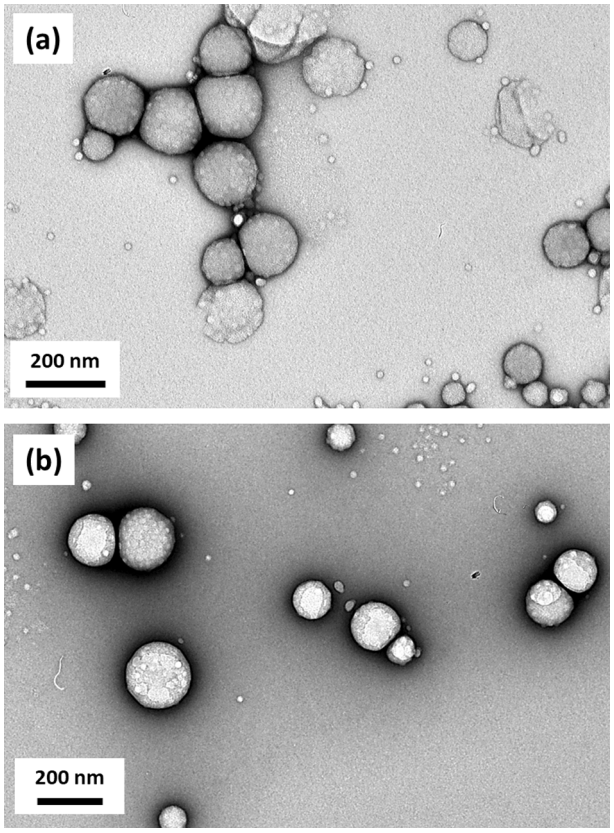

Fig. 4. Representative TEM images obtained after drying squalane-in-water Pickering nanoemulsions prepared using (a) hydroxyl-functional PGEO5MA$_{26}$-PTFEMA$_{35}$ nanoparticles and (b) aldehyde-functional PGEO5MA$_{26}$-PTFEMA$_{35}$ nanoparticles. In each case, the squalane and water are removed under the ultrahigh vacuum conditions required for TEM studies, leaving the nanoparticle superstructure that originally surrounded each oil droplet.

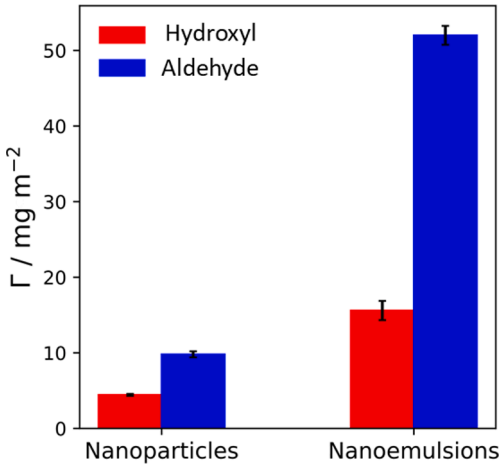

Fig. 5. Adsorbed amount, Γ, calculated for hydroxyl (red) or aldehyde (blue) functionalized nanoparticles and the corresponding nanoparticle-coated squalane droplets on model primary amine-functionalized planar substrates as determined by QCM. The Δ*f* vs. time raw data plots are shown in Figure S8. (For interpretation of the references to color in this figure legend, the reader is referred to the web version of this article.)

substrate than the corresponding hydroxyl-functional nanoparticles. More specifically, Γ = 9.8 mg m^{-2} for the former nanoparticles, whereas Γ = 4.4 mg m^{-2} for the latter. These findings are consistent with tapping mode AFM images obtained for these two types of nanoparticles adsorbed onto aminated silicon wafers (see Figure S9). Furthermore, the adsorbed amount obtained for the corresponding aldehyde-functional squalane droplets (Γ = 52 mg m^{-2}) is more than three times higher than that obtained for the hydroxyl-functional squalane droplets (Γ = 16 mg m^{-2}). Hence appropriate surface functionality of the oil droplets profoundly affects their adsorption at a model planar surface bearing primary amine groups. The important remaining question is whether such 2D data can be used to predict mucoadhesion performance within a 3D environment.

3.1. *Retention of nanoparticles on sheep nasal mucosa*

Retention of the Nile Red-labeled squalane droplets prepared using either aldehyde- or hydroxyl-functionalized nanoparticles on sheep nasal mucosa was examined using an assay based on flow-through fluorescence microscopy. Representative fluorescence images recorded for all samples after washing with ANF at various time points are shown in Figure 6 and the corresponding fluorescence intensities are presented in Figure 7. Clearly, the aldehyde-functionalized squalane droplets exhibit significantly greater retention on sheep nasal mucosa compared to the corresponding hydroxyl-functionalized squalane droplets. Indeed, mucoadhesion of the former droplets is comparable to that exhibited by chitosan, which is widely regarded as a gold standard in this context. [58,62] This is because the aldehyde groups at the surface of the adsorbed nanoparticles that surround each oil droplet (see Figure 3) can

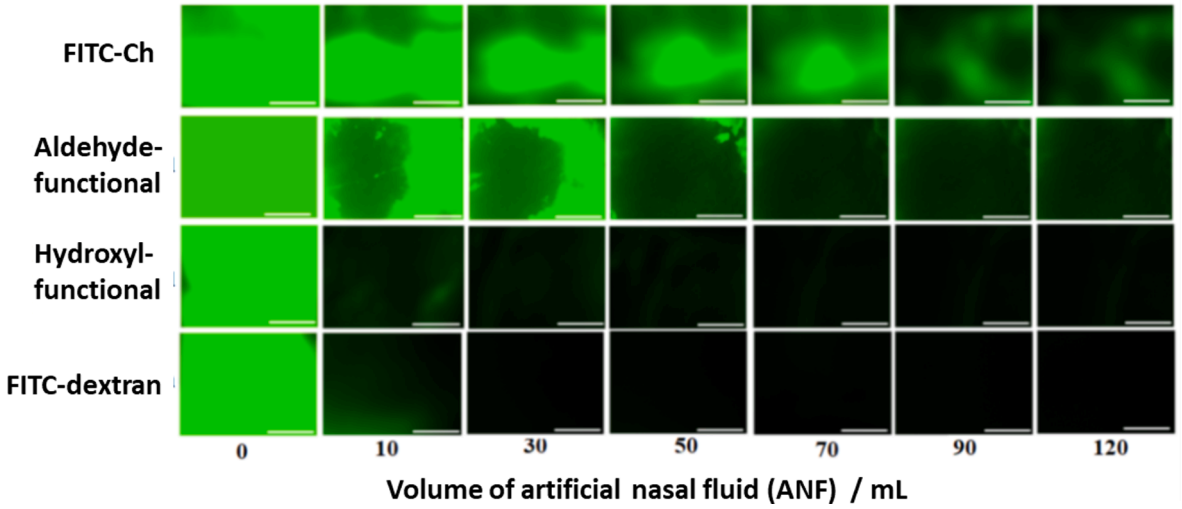

Fig. 6. Representative fluorescence images showing the retention of Nile Red-labeled squalane droplets prepared using either aldehyde- or hydroxyl-functionalized nanoparticles on freshly-excised sheep nasal mucosa, along with FITC-chitosan and FITC-dextran (which serve as positive and negative controls, respectively). Images were recorded at various time points during tissue washing with varying volumes of artificial nasal fluid (ANF) at a flow rate of 1 mL min^{-1}. The scale bar represents 2 mm. [N.B. Images of sheep nasal mucosa after exposure to Nile Red-labeled squalane droplets were recorded using a different microscope filter and were converted to a green color for consistency with the controls]. (For interpretation of the references to color in this figure legend, the reader is referred to the web version of this article.)

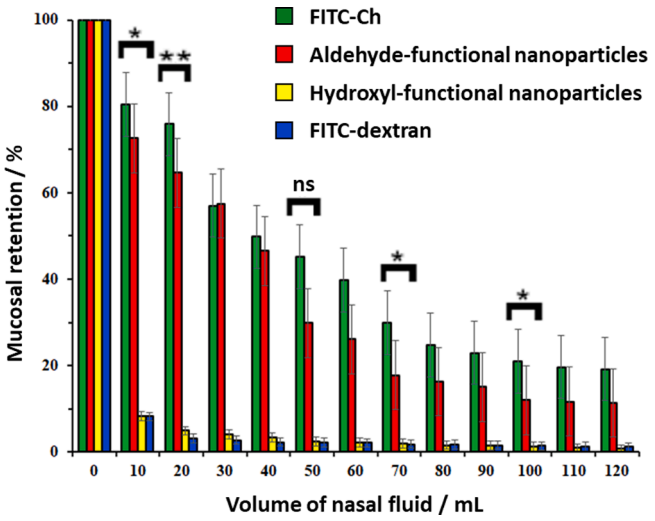

Fig. 7. Relative retention data obtained for Nile Red-labeled squalane droplets functionalized with either surface aldehyde or hydroxyl groups, FITC-chitosan (positive control) and FITC-dextran (negative control) when using freshly-excised sheep nasal mucosa as a model substrate. Data are expressed as mean ± SD (n =3). * denotes $p < 0.05$, ** denotes $p < 0.01$, and 'ns' denotes no significance. (For interpretation of the references to color in this figure legend, the reader is referred to the web version of this article.)

form imine bonds with amine groups on the mucosal surface via Schiff base chemistry.[86] In striking contrast, hydroxyl-functionalized squalane droplets exhibit poor retention on the nasal mucosa, just like the FITC-dextran negative control. Indeed, the non-mucoadhesive nature of hydroxyl-rich dextran is widely recognized in the literature.[86–88]

4. Toxicological studies

4.1. Toxicity assay against planaria

Planaria is a freshwater flatworm that serves as a useful model organism to assess the toxicological profiles of various chemicals. Recently, we reported the use of planaria for the rapid pre-screening of potential skin irritants.[71] Two methods were employed to evaluate the toxicity and irritation potential of each nanoemulsion. The first method involved direct exposure of planaria to the aqueous nanoemulsion (at either 0.5 g or 1.0 dm^{-3}) for up to 48 h, followed by assessment of this organism's viability and behavior. This is an acute test designed to reveal strong toxicological effects that may result in death of the organism. The results are summarized in Figure S10. Two concentrations of a known strong irritant (benzalkonium chloride, BC) were used as a positive control and APW was used as a negative control. As expected, exposure of planaria to BC resulted in 100% morbidity with significant bodily deformation. In contrast, all planaria survived 48 h exposure to APW and also to each nanoemulsion (at both concentrations). This suggests that these nanoemulsions are relatively safe materials that have minimal adverse effects on this organism.

4.2. Fluorescence intensity studies

The epithelial surface of all biological organisms acts as a protective barrier. When such epithelial layers are exposed to irritant chemicals, they can become damaged and hence more permeable, allowing their penetration by small molecules. This is the underlying principle for the planarian toxicity fluorescence assay recently developed by Khutoryanskiy and co-workers as a pre-screening tool to identify potential skin irritants.[71] Thus, planaria are initially exposed to the test chemical for a given time period. After gentle washing, the worms are placed into an aqueous solution of sodium fluorescein, with subsequent penetration of this water-soluble dye being assessed by fluorescence microscopy.

Empirically, it was found that using a BC concentration of 0.1 g dm^{-3} and a contact time of 1 min per worm produced high-quality fluorescence images (see Experimental and Figure S11). Subsequently, all the planaria used for the acute toxicity test were exposed to a 0.1% w/v aqueous solution of sodium fluorescein (NaFl) for 1 min to evaluate the barrier properties conferred by their epithelia. The corresponding fluorescence images for such planaria are shown in Figure 8. Clearly, exposure to benzalkonium chloride (positive control) enables NaFl to penetrate deeply into the planaria and stain this organism more efficiently. In contrast, planaria exposed to APW (negative control), the hydroxyl-functional nanoemulsion or the aldehyde-functionalized nanoemulsion do not suffer substantial dye penetration – instead the fluorescent probe is mainly located at the surface of each organism.

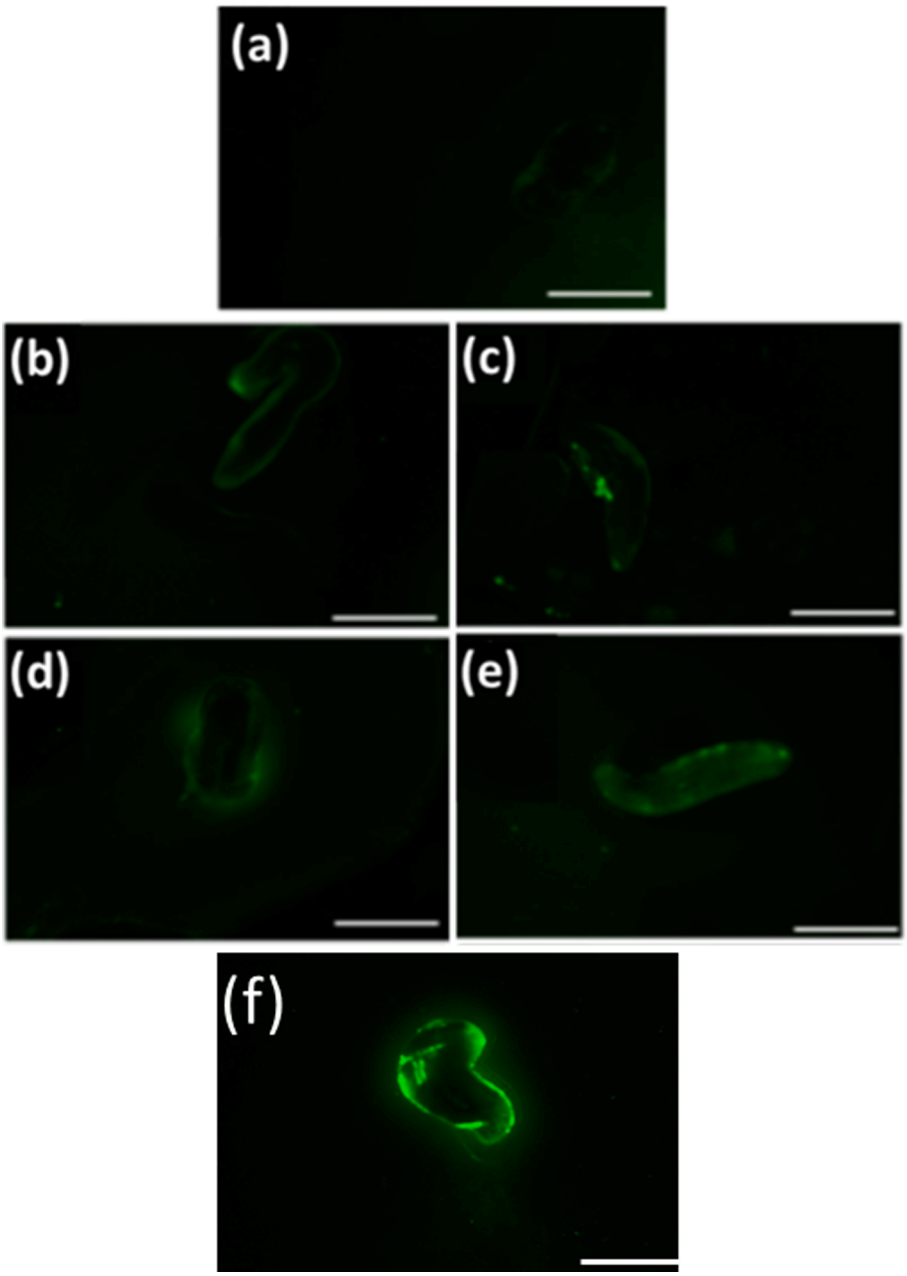

Fig. 8. Representative fluorescence images recorded for planaria after exposure to: (a) a negative control (artificial pond water, APW); the hydroxyl-functionalized nanoemulsion at (b) 0.5 g dm^{-3} and (c) 1.0 g dm^{-3}; the aldehyde-functionalized nanoemulsion at (d) 0.5 g dm^{-3} and (e) 1.0 g dm^{-3}, and a positive control (benzalkonium chloride, BC) at (f) 0.1. The scale bar represents 2 mm.

Figure 9 shows the data derived from quantitative analysis of the fluorescence images. As expected, the lowest fluorescence intensity (6.7 ± 0.9 a.u. cm^{-2}) was observed for planaria exposed to the negative control (APW). Exposure of planaria to the hydroxyl-functionalized nanoemulsion at 0.5 or 1.0 g dm^{-3} produced comparable fluorescence intensities of 9.2 ± 0.8 a.u. cm^{-2} and 12.2 ± 1.2 a.u. cm^{-2}, respectively. Indeed, these values are not statistically significantly different from the APW data, which indicates that this nanoemulsion does not cause any discernible irritancy to this organism. However, the fluorescence intensity data obtained for the aldehyde-functionalized nanoemulsion indicated slightly higher values of 11.1 ± 0.5 a.u. cm^{-2} and 15.2 ± 0.6 a.u. cm^{-2} when used at concentrations of 0.5 or 1.0 g dm^{-3} respectively, and this difference is statistically significant ($p < 0.05$). This suggests that this nanoemulsion most likely causes minor irritation, but further experiments are required to study its toxicological profile in more detail. Finally, the fluorescence intensities recorded for planaria exposed to a strong irritant (BC) are very high (82.5 ± 5.8 a.u. cm^{-2} and 87.9 ± 4.8 a.u. cm^{-2} for 0.5 and 1.0 g dm^{-3} BC, respectively). This positive control indicates that neither nanoemulsion is a strong irritant, at least with regard to planaria.

5. Conclusions

In summary, new aldehyde-functionalized sterically-stabilized diblock copolymer nanoparticles of 20 nm diameter are prepared by selective oxidation of precursor hydroxyl-functional diblock copolymer nanoparticles using sodium periodate. Both types of nanoparticles are used to prepare oil-in-water Pickering nanoemulsions via high-pressure microfluidization with a mean droplet diameter of approximately 200 nm being obtained in each case. The oil was chosen to be squalane,

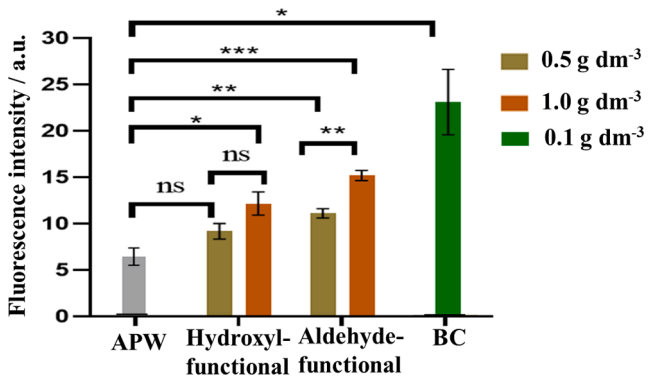

Fig. 9. Fluorescence intensity per unit area (cm^2) of planaria after exposure to a negative control (artificial pond water, APW), the hydroxyl-functionalized nanoemulsion, the aldehyde-functionalized nanoemulsion, and 0.1 g dm^{-3} of a positive control (benzalkonium chloride, BC). Data are expressed as mean ± SD (n = 3), where * denotes $p < 0.05$, ** denotes $p < 0.01$, *** denotes $p < 0.001$ and 'ns' denotes no significance.

which is highly biocompatible and has sufficiently low aqueous solubility to suppress Ostwald ripening [26]. Our QCM studies confirmed that both the aldehyde-functionalized nanoparticles and the corresponding nanoparticle-coated squalane droplets exhibited significantly stronger adsorption onto a model aminated planar substrate compared to the precursor hydroxyl-functional nanoparticles and squalane droplets. Such differences are attributed to the formation of surface imine bonds. These observations are consistent with the enhanced adsorption of squalane droplets (prepared using the aldehyde-functional nanoparticles) onto freshly excised sheep nasal mucosa, as judged by a fluorescence microscopy flow-through assay. Preliminary assays performed using planaria indicate only mild toxicity for such Pickering nanoemulsions, which suggests that they may offer a potential new vehicle for the targeted delivery of *hydrophobic* drugs via a mucoadhesion strategy. Hence these nanoemulsions differ significantly from the mucoadhesive worm gels recently reported by us, [65] which in principle can be used for the localized delivery of *hydrophilic* drugs, globular proteins or enzymes. This study makes a useful contribution to the fast-growing field of Pickering nanoemulsions by (i) providing a rare example of a relatively stable formulation and (ii) demonstrating that appropriate surface functionality leads to enhanced interfacial adsorption.

Declaration of Competing Interest

The authors declare the following financial interests/personal relationships which may be considered as potential competing interests: Steven P. Armes (salary) and Saul J. Hunter (PhD stipend) reports financial support was provided by Engineering and Physical Sciences Research Council. Steven P. Armes reports financial support and equipment, drugs, or supplies were provided by GEO Specialty Chemicals Inc Southampton. Vitaliy Khutoryanskiy reports financial support was provided by The Royal Society.

Data availability

Data will be made available on request.

Acknowledgments

S.P.A. thanks EPSRC for an Established Career Particle Technology Fellowship (EP/R003009/01) which supported S.J.H. EPSRC is acknowledged for a CDT studentship for E.E.B. (EP/L016281/1). GEO Specialty Chemicals (Hythe, UK) is acknowledged for additional financial support, supply of the GEO5MA monomer and for permission to publish this work. V.V.K. thanks the Royal Society for a Royal Society Industry Fellowship (IF/R2/222031). Myrale Habel is gratefully acknowledged for establishing and maintaining planaria culture at the Reading School of Pharmacy.

Appendix A. Supplementary data

Reaction schemes for the synthesis of the $PGEO5MA_{26}$ precursor, ^{19}F NMR spectrum recorded for the $PGEO5MA_{26}$-$PTFEMA_{35}$ diblock copolymer, GPC curves and ^{1}H NMR spectra recorded for the $PGEO5MA_{26}$ precursor and the corresponding $PGEO5MA_{26}$–$PTFEMA_{35}$ and $PAGEO5MA_{26}$–$PTFEMA_{35}$, laser diffraction droplet size distributions for Pickering macroemulsions, Droplet size distributions for Pickering nanoemulsions, raw Δf vs. time plots, acute toxicity assay, optimization of the planarian toxicity fluorescent assay with a suitable positive control. Supplementary data to this article can be found online at https://doi.org/10.1016/j.jcis. Supplementary data to this article can be found online at https://doi.org/10.1016/j.jcis.2023.07.162.

References

[1] B.P. Binks, J.H. Clint, P.D.I. Fletcher, S. Rippon, S.D. Lubetkin, P.J. Mulqueen, Kinetics of Swelling of Oil-in-Water Emulsions Stabilized by Different Surfactants, Langmuir 15 (1999) 4495–4501.
[2] B.P. Binks, S.O. Lumsdon, Stability of oil-in-water emulsions stabilised by silica particles, PCCP 1 (1999) 3007–3016.
[3] B.P. Binks, S.O. Lumsdon, Influence of Particle Wettability on the Type and Stability of Surfactant-Free Emulsions, Langmuir 16 (2000) 8622–8631.
[4] B.P. Binks, S.O. Lumsdon, Catastrophic Phase Inversion of Water-in-Oil Emulsions Stabilized by Hydrophobic Silica, Langmuir 16 (2000) 2539–2547.
[5] B.P. Binks, S.O. Lumsdon, Pickering Emulsions Stabilized by Monodisperse Latex Particles: Effects of Particle Size, Langmuir 17 (2001) 4540–4547.
[6] B.P. Binks, Particles as surfactants—similarities and differences, Curr. Opin. Colloid Interface Sci. 7 (2002) 21–41.
[7] R. Aveyard, B.P. Binks, J.H. Clint, Emulsions stabilised solely by colloidal particles, Adv. Colloid Interface Sci. 100 (2003) 503–546.
[8] S. Arditty, C.P. Whitby, B.P. Binks, V. Schmitt, F. Leal-Calderon, Some general features of limited coalescence in solid-stabilized emulsions, The, European Physical Journal E 11 (2003) 273–281.
[9] B.P. Binks, C.P. Whitby, Nanoparticle silica-stabilised oil-in-water emulsions: improving emulsion stability, Colloids Surf A Physicochem Eng Asp 253 (2005) 105–115.
[10] S. Fujii, E.S. Read, B.P. Binks, S.P. Armes, Stimulus-Responsive Emulsifiers Based on Nanocomposite Microgel Particles, Adv. Mater. 17 (2005) 1014–1018.
[11] S. Fujii, S.P. Armes, B.P. Binks, R. Murakami, Stimulus-Responsive Particulate Emulsifiers Based on Lightly Cross-Linked Poly(4-vinylpyridine)−Silica Nanocomposite Microgels, Langmuir 22 (2006) 6818–6825.
[12] W. Ramsden, Separation of Solids in the Surface-Layers of Solutions and 'Suspensions' (Observations on Surface-Membranes, Bubbles, Emulsions, and Mechanical Coagulation).–Preliminary Account, Proc. R. Soc. Lond. 72 (1903) 156–164.
[13] S.U. Pickering, Emulsions, J. Chem. Soc. Trans. 91 (1907) 2001–2021.
[14] B.P. Binks, C.P. Whitby, Silica Particle-Stabilized Emulsions of Silicone Oil and Water: Aspects of Emulsification, Langmuir 20 (2004) 1130–1137.
[15] A. Menner, V. Ikem, M. Salgueiro, M.S.P. Shaffer, A. Bismarck, High internal phase emulsion templates solely stabilised by functionalised titania nanoparticles, Chem. Commun. 4274–4276 (2007).
[16] N.P. Ashby, B.P. Binks, Pickering emulsions stabilised by Laponite clay particles, PCCP 2 (2000) 5640–5646.
[17] I. Kalashnikova, H. Bizot, B. Cathala, I. Capron, New Pickering Emulsions Stabilized by Bacterial Cellulose Nanocrystals, Langmuir 27 (2011) 7471–7479.
[18] A. Saha, A. Nikova, P. Venkataraman, V.T. John, A. Bose, Oil Emulsification Using Surface-Tunable Carbon Black Particles, ACS Appl. Mater. Interfaces 5 (2013) 3094–3100.
[19] J. Kim, L.J. Cote, F. Kim, W. Yuan, K.R. Shull, J.X. Huang, Graphene Oxide Sheets at Interfaces, J. Am. Chem. Soc. 132 (2010) 8180–8186.
[20] S.J. Hunter, S.P. Armes, Pickering Emulsifiers Based on Block Copolymer Nanoparticles Prepared by Polymerization-Induced Self-Assembly, Langmuir 36 (2020) 15463–15484.
[21] R. Gupta, D. Rousseau, Surface-active solid lipid nanoparticles as Pickering stabilizers for oil-in-water emulsions, Food Funct. 3 (2012) 302–311.
[22] S. Sihler, A. Schrade, Z. Cao, U. Ziener, Inverse Pickering Emulsions with Droplet Sizes below 500 nm, Langmuir 31 (2015) 10392–10401.
[23] K.H. Persson, I.A. Blute, I.C. Mira, J. Gustafsson, Creation of well-defined particle stabilized oil-in-water nanoemulsions, Colloids Surf A Physicochem Eng Asp 459 (2014) 48–57.
[24] K.L. Thompson, N. Cinotti, E.R. Jones, C.J. Mable, P.W. Fowler, S.P. Armes, Bespoke Diblock Copolymer Nanoparticles Enable the Production of Relatively Stable Oil-in-Water Pickering Nanoemulsions, Langmuir 33 (2017) 12616–12623.

[25] D.J. Kang, H. Bararnia, S. Anand, Synthesizing Pickering Nanoemulsions by Vapor Condensation, ACS Appl. Mater. Interfaces 10 (2018) 21746–21754.
[26] K.L. Thompson, M.J. Derry, F.L. Hatton, S.P. Armes, Long-Term Stability of n-Alkane-in-Water Pickering Nanoemulsions: Effect of Aqueous Solubility of Droplet Phase on Ostwald Ripening, Langmuir 34 (2018) 9289–9297.
[27] C. Jiménez Saelices, I. Capron, Design of Pickering Micro- and Nanoemulsions Based on the Structural Characteristics of Nanocelluloses, Biomacromolecules 19 (2018) 460–469.
[28] Z. Du, Q. Li, J. Li, E. Su, X. Liu, Z. Wan, X. Yang, Self-Assembled Egg Yolk Peptide Micellar Nanoparticles as a Versatile Emulsifier for Food-Grade Oil-in-Water Pickering Nanoemulsions, J. Agric. Food Chem. 67 (2019) 11728–11740.
[29] Q. Zhao, L.X. Jiang, Z. Lian, E. Khoshdel, S. Schumm, J.B. Huang, Q.Q. Zhang, High internal phase water-in-oil emulsions stabilized by food-grade starch, J. Colloid Interface Sci. 534 (2019) 542–548.
[30] S.J. Hunter, E.J. Cornel, O.O. Mykhaylyk, S.P. Armes, Effect of Salt on the Formation and Stability of Water-in-Oil Pickering Nanoemulsions Stabilized by Diblock Copolymer Nanoparticles, Langmuir 36 (2020) 15523–15535.
[31] S.J. Hunter, S.P. Armes, Long-Term Stability of Pickering Nanoemulsions Prepared Using Diblock Copolymer Nanoparticles: Effect of Nanoparticle Core Crosslinking, Oil Type, and the Role Played by Excess Copolymers, Langmuir 38 (2022) 8021–8029.
[32] M. Nandy, B.B. Lahiri, J. Philip, Inter-droplet force between magnetically polarizable Pickering oil-in-water nanoemulsions stabilized with γ-Al2O3 nanoparticles: Role of electrostatic and electric dipolar interactions, J. Colloid Interface Sci. 607 (2022) 1671–1686.
[33] D.J. McClements, Nanoemulsions versus microemulsions: terminology, differences, and similarities, Soft Matter 8 (2012) 1719–1729.
[34] C. Solans, P. Izquierdo, J. Nolla, N. Azemar, M.J. Garcia-Celma, Nano-emulsions, Curr. Opin. Colloid Interface Sci. 10 (2005) 102–110.
[35] K.L. Thompson, C.J. Mable, A. Cockram, N.J. Warren, V.J. Cunningham, E. R. Jones, R. Verber, S.P. Armes, Are block copolymer worms more effective Pickering emulsifiers than block copolymer spheres? Soft Matter 10 (2014) 8615–8626.
[36] C.J. Mable, N.J. Warren, K.L. Thompson, O.O. Mykhaylyk, S.P. Armes, Framboidal ABC triblock copolymer vesicles: a new class of efficient Pickering emulsifier, Chem. Sci. 6 (2015) 6179–6188.
[37] M. Porras, C. Solans, C. González, A. Martínez, A. Guinart, J.M. Gutiérrez, Studies of formation of W/O nano-emulsions, Colloids Surf, A 249 (2004) 115–118.
[38] P. Izquierdo, J. Feng, J. Esquena, T.F. Tadros, J.C. Dederen, M.J. Garcia, N. Azemar, C. Solans, The influence of surfactant mixing ratio on nano-emulsion formation by the pit method, J Colloid Interface Sci 285 (2005) 388–394.
[39] I. Solè, A. Maestro, C.M. Pey, C. González, C. Solans, J.M. Gutiérrez, Nano-emulsions preparation by low energy methods in an ionic surfactant system, Colloids Surf, A 288 (2006) 138–143.
[40] T.J. Wooster, M. Golding, P. Sanguansri, Impact of Oil Type on Nanoemulsion Formation and Ostwald Ripening Stability, Langmuir 24 (2008) 12758–12765.
[41] G. Rodriguez-Lopez, Y. O'Neil Williams, J. Toro-Mendoza, Individual and Collective Behavior of Emulsion Droplets Undergoing Ostwald Ripening, Langmuir 35 (2019) 5316–5323.
[42] S.J. Hunter, N.J.W. Penfold, D.H. Chan, O.O. Mykhaylyk, S.P. Armes, How Do Charged End-Groups on the Steric Stabilizer Block Influence the Formation and Long-Term Stability of Pickering Nanoemulsions Prepared Using Sterically Stabilized Diblock Copolymer Nanoparticles? Langmuir 36 (2020) 769–780.
[43] A. Gupta, H.B. Eral, T.A. Hatton, P.S. Doyle, Nanoemulsions: formation, properties and applications, Soft Matter 12 (2016) 2826–2841.
[44] N.J. Warren, S.P. Armes, Polymerization-Induced Self-Assembly of Block Copolymer Nano-objects via RAFT Aqueous Dispersion Polymerization, J. Am. Chem. Soc. 136 (2014) 10174–10185.
[45] A.B. Lowe, RAFT alcoholic dispersion polymerization with polymerization-induced self-assembly, Polymer 106 (2016) 161–181.
[46] M.J. Derry, L.A. Fielding, S.P. Armes, Polymerization-induced self-assembly of block copolymer nanoparticles via RAFT non-aqueous dispersion polymerization, Prog. Polym. Sci. 52 (2016) 1–18.
[47] J. Rieger, Guidelines for the Synthesis of Block Copolymer Particles of Various Morphologies by RAFT Dispersion Polymerization, Macromol. Rapid Commun. 36 (2015) 1458–1471.
[48] B. Charleux, G. Delaittre, J. Rieger, F. D'Agosto, Polymerization-Induced Self-Assembly: From Soluble Macromolecules to Block Copolymer Nano-Objects in One Step, Macromolecules 45 (2012) 6753–6765.
[49] F. D'Agosto, J. Rieger, M. Lansalot, RAFT-Mediated Polymerization-Induced Self-Assembly, Angew. Chem. Int. Ed. 59 (2020) 8368–8392.
[50] N.J.W. Penfold, J. Yeow, C. Boyer, S.P. Armes, Emerging Trends in Polymerization-Induced Self-Assembly, ACS Macro Lett. 8 (2019) 1029–1054.
[51] V.J. Cunningham, A.M. Alswieleh, K.L. Thompson, M. Williams, G.J. Leggett, S. P. Armes, O.M. Musa, Poly(glycerol monomethacrylate)–Poly(benzyl methacrylate) Diblock Copolymer Nanoparticles via RAFT Emulsion Polymerization: Synthesis, Characterization, and Interfacial Activity, Macromolecules 47 (2014) 5613–5623.
[52] B. Akpinar, L.A. Fielding, V.J. Cunningham, Y. Ning, O.O. Mykhaylyk, P.W. Fowler, S.P. Armes, Determining the Effective Density and Stabilizer Layer Thickness of Sterically Stabilized Nanoparticles, Macromolecules 49 (2016) 5160–5171.
[53] F.L. Hatton, J.R. Lovett, S.P. Armes, Synthesis of well-defined epoxy-functional spherical nanoparticles by RAFT aqueous emulsion polymerization, Polym. Chem. 8 (2017) 4856–4868.
[54] F. Laffleur, A. Bernkop-Schnürch, Strategies for improving mucosal drug delivery, Nanomedicine 8 (2013) 2061–2075.
[55] S. Gänger, K. Schindowski, Tailoring Formulations for Intranasal Nose-to-Brain Delivery: A Review on Architecture, Physico-Chemical Characteristics and Mucociliary Clearance of the Nasal Olfactory Mucosa, Pharmaceutics 10 (2018) 116.
[56] N.A. Peppas, J.J. Sahlin, Hydrogels as mucoadhesive and bioadhesive materials: a review, Biomaterials 17 (1996) 1553–1561.
[57] I.S. Bayer, Recent Advances in Mucoadhesive Interface Materials, Mucoadhesion Characterization, and Technologies, Advanced Materials, Interfaces 9 (2022) 2200211.
[58] V.V. Khutoryanskiy, Advances in Mucoadhesion and Mucoadhesive Polymers, Macromol. Biosci. 11 (2011) 748–764.
[59] R.P. Brannigan, V.V. Khutoryanskiy, Progress and Current Trends in the Synthesis of Novel Polymers with Enhanced Mucoadhesive Properties, Macromol. Biosci. 19 (2019) 1900194.
[60] M. Surendranath, R.M. R, R. Parameswaran, Recent advances in functionally modified polymers for mucoadhesive drug delivery, J. Mater. Chem. B 10 (2022) 5913–5924.
[61] G.S. Irmukhametova, G.A. Mun, V.V. Khutoryanskiy, Thiolated Mucoadhesive and PEGylated Nonmucoadhesive Organosilica Nanoparticles from 3-Mercaptopropyltrimethoxysilane, Langmuir 27 (2011) 9551–9556.
[62] P. Tonglairoum, R.P. Brannigan, P. Opanasopit, V.V. Khutoryanskiy, Maleimide-bearing nanogels as novel mucoadhesive materials for drug delivery, J. Mater. Chem. B 4 (2016) 6581–6587.
[63] M.T. Cook, G. Tzortzis, D. Charalampopoulos, V.V. Khutoryanskiy, Production and Evaluation of Dry Alginate-Chitosan Microcapsules as an Enteric Delivery Vehicle for Probiotic Bacteria, Biomacromolecules 12 (2011) 2834–2840.
[64] S.E. Edwards, S. Flynn, J.J. Hobson, P. Chambon, H. Cauldbeck, S.P. Rannard, Mucus-responsive functionalized emulsions: design, synthesis and study of novel branched polymers as functional emulsifiers, RSC Adv. 10 (2020) 30463–30475.
[65] E.E. Brotherton, T.J. Neal, D.B. Kaldybekov, M.J. Smallridge, V.V. Khutoryanskiy, S.P. Armes, Aldehyde-functional thermoresponsive diblock copolymer worm gels exhibit strong mucoadhesion, Chem. Sci. 13 (2022) 6888–6898.
[66] E. Tellechea, D. Johannsmann, N.F. Steinmetz, R.P. Richter, I. Reviakine, Model-Independent Analysis of QCM Data on Colloidal Particle Adsorption, Langmuir 25 (2009) 5177–5184.
[67] Z. Adamczyk, M. Sadowska, P. Żeliszewska, Applicability of QCM-D for Quantitative Measurements of Nano- and Microparticle Deposition Kinetics: Theoretical Modeling and Experiments, Anal. Chem. 92 (2020) 15087–15095.
[68] A.D. Easley, T. Ma, C.I. Eneh, J. Yun, R.M. Thakur, J.L. Lutkenhaus, A practical guide to quartz crystal microbalance with dissipation monitoring of thin polymer films, J. Polym. Sci. 60 (2022) 1090–1107.
[69] M.d.S. Barbi, F.C. Carvalho, C.P. Kiill, H. Da Silva Barud, S.H. Santagneli, S.J. L. Ribeiro, M.P.D. Gremião, Preparation and Characterization of Chitosan Nanoparticles for Zidovudine Nasal Delivery, J. Nanosci. Nanotechnol. 15 (2015) 865–874.
[70] N.N. Porfiryeva, S.F. Nasibullin, S.G. Abdullina, I.K. Tukhbatullina, R. I. Moustafine, V.V. Khutoryanskiy, Acrylated Eudragit® E PO as a novel polymeric excipient with enhanced mucoadhesive properties for application in nasal drug delivery, Int. J. Pharm. 562 (2019) 241–248.
[71] S.I. Shah, A.C. Williams, W.M. Lau, V.V. Khutoryanskiy, Planarian toxicity fluorescent assay: A rapid and cheap pre-screening tool for potential skin irritants, Toxicol. In Vitro 69 (2020), 105004.
[72] D.H.H. Chan, S.J. Hunter, T.J. Neal, C. Lindsay, P. Taylor, S.P. Armes, Adsorption of sterically-stabilized diblock copolymer nanoparticles at the oil–water interface: effect of charged end-groups on interfacial rheology, Soft Matter 18 (2022) 6757–6770.
[73] E.E. Brotherton, C.P. Jesson, N.J. Warren, M.J. Smallridge, S.P. Armes, New Aldehyde-Functional Methacrylic Water-Soluble Polymers, Angew. Chem. Int. Ed. 60 (2021) 12032–12037.
[74] E.E. Brotherton, M.J. Smallridge, S.P. Armes, Aldehyde-Functional Diblock Copolymer Nano-objects via RAFT Aqueous Dispersion Polymerization, Biomacromolecules 22 (2021) 5382–5389.
[75] T. Serizawa, S. Kamimura, M. Akashi, Electrostatic adsorption of polystyrene particles with different surface charges onto the surface of an ultrathin polymer film, Colloids Surf A Physicochem Eng Asp 164 (2000) 237–245.
[76] Y. Yan, X. Zhou, J. Ji, L. Yan, G. Zhang, Adsorption of Polymeric Micelles and Vesicles on a Surface Investigated by Quartz Crystal Microbalance, J. Phys. Chem. B 110 (2006) 21055–21059.
[77] F. Sebastiani, M. Yanez Arteta, L. Lindfors, M. Cárdenas, Screening of the binding affinity of serum proteins to lipid nanoparticles in a cell free environment, J. Colloid Interface Sci. 610 (2022) 766–774.
[78] K. Sakai, E.G. Smith, G.B. Webber, C. Schatz, E.J. Wanless, V. Bütün, S.P. Armes, S. Biggs, pH-Responsive Diblock Copolymer Micelles at the Silica/Aqueous Solution Interface: Adsorption Kinetics and Equilibrium Studies, J. Phys. Chem. B 110 (2006) 14744–14753.
[79] K.V. Tretiakov, K.J.M. Bishop, B. Kowalczyk, A. Jaiswal, M.A. Poggi, B. A. Grzybowski, Mechanism of the Cooperative Adsorption of Oppositely Charged Nanoparticles, Chem. A Eur. J. 113 (2009) 3799–3803.
[80] D. Xu, C. Hodges, Y. Ding, S. Biggs, A. Brooker, D. York, A QCM Study on the Adsorption of Colloidal Laponite at the Solid/Liquid Interface, Langmuir 26 (2010) 8366–8372.
[81] L.V. Sigolaeva, U. Günther, D.V. Pergushov, S.Y. Gladyr, I.N. Kurochkin, F. H. Schacher, Sequential pH-Dependent Adsorption of Ionic Amphiphilic Diblock Copolymer Micelles and Choline Oxidase Onto Conductive Substrates: Toward the Design of Biosensors, Macromol. Biosci. 14 (2014) 1039–1051.

[82] Q. Chen, S. Xu, Q. Liu, J. Masliyah, Z. Xu, QCM-D study of nanoparticle interactions, Adv. Colloid Interface Sci. 233 (2016) 94–114.
[83] J. Engström, M.S. Reid, E.E. Brotherton, E. Malmström, S.P. Armes, F.L. Hatton, Investigating the adsorption of anisotropic diblock copolymer worms onto planar silica and nanocellulose surfaces using a quartz crystal microbalance, Polym. Chem. 12 (2021) 6088–6100.
[84] J. Engström, T. Benselfelt, L. Wågberg, F. D'Agosto, M. Lansalot, A. Carlmark, E. Malmström, Tailoring adhesion of anionic surfaces using cationic PISA-latexes – towards tough nanocellulose materials in the wet state, Nanoscale 11 (2019) 4287–4302.
[85] C. György, P.M. Kirkman, T.J. Neal, D.H.H. Chan, M. Williams, T. Smith, D. J. Growney, S.P. Armes, Enhanced Adsorption of Epoxy-Functional Nanoparticles onto Stainless Steel Significantly Reduces Friction in Tribological Studies, Angew. Chem. Int. Ed. 62 (2023) e202218397.
[86] A. Štorha, E.A. Mun, V.V. Khutoryanskiy, Synthesis of thiolated and acrylated nanoparticles using thiol-ene click chemistry: towards novel mucoadhesive materials for drug delivery, RSC Adv. 3 (2013) 12275–12279.
[87] C.A. Withers, M.T. Cook, L. Methven, M.A. Gosney, V.V. Khutoryanskiy, Investigation of milk proteins binding to the oral mucosa, Food Funct. 4 (2013) 1668–1674.
[88] E.A. Mun, A.C. Williams, V.V. Khutoryanskiy, Adhesion of thiolated silica nanoparticles to urinary bladder mucosa: Effects of PEGylation, thiol content and particle size, Int. J. Pharm. 512 (2016) 32–38.